Catalysis Science & Technology

PAPER

View Article Online
View Journal | View Issue

Cite this: *Catal. Sci. Technol.*, 2019, 9, 3820

Engineering of highly active Au/Pd supported on hydrogenated urchin-like yolk@shell TiO_2 for visible light photocatalytic Suzuki coupling†

Sahar Rohani, [ab] Abolfazl Ziarati, [bc] Ghodsi Mohammadi Ziarani, [a] Alireza Badiei [c] and Thomas Burgi *[b]

Efficient smart photocatalysts and their surface engineering are necessary for the effective conversion of light energy into chemical energy in photocatalyzed organic reactions. Herein, we designed a hydrogenated urchin-like yolk@shell TiO_2 structure decorated with Au and Pd nanoparticles (HUY@S-TOH@AuPd) as a robust photocatalyst for C–C coupling reactions. The resulting architecture exhibits considerable photocatalytic performance in Suzuki coupling reactions under visible light irradiation with a turnover frequency (TOF) value as high as 7095 h^{-1}. The beauty of this engineered structure lies on the following four points: (I) the urchin-like structure provided a large accessible surface area for high light harvesting as well as high noble metal anchoring; (II) the yolk@shell mesoporous architecture improved the absorption of light by multiple scattering; (III) the presence of Ti^{3+} species on the surface of TiO_2 decreased the band gap of the structure to the visible region; (IV) the enriched electron density of Pd through the injection of hot electrons from Au as well as the flow of electrons from the titanium dioxide semiconductor to the metals accelerated the rate-determining step. The merging of bimetallic plasmonic nanoparticles and urchin like yolk–shell hydrogenated titanium dioxide architecture can open an avenue for designing photocatalysts with high stability and promising activity as well as high direct harvesting of visible light for a broad range of photocatalytic organic reactions.

Received 26th April 2019,
Accepted 23rd June 2019

DOI: 10.1039/c9cy00798a

rsc.li/catalysis

Introduction

The development of environmentally friendly photocatalytic materials for organic molecular transformations with high activity and stability under mild conditions is of great importance for both fundamental research and practical applications.[1,2] One special focus is on the use of photo-induced electrons/holes for reduction/oxidation of organic molecules.[3,4] Despite the fact that the simultaneous application of photo-excited electrons and holes for organic reactions offers a novel and promising catalytic strategy for economical and green chemical synthesis, it is rarely reported and still a challenge for the scientific community.[5,6] Suzuki–Miyaura coupling is one of the most powerful tools in modern organic synthesis for C–C bond formation.[7–9] The photocatalytic Suzuki reaction driven by visible light is an ideal procedure, due to its clean and abundant energy source, benign environmental impact and sustainability.[10–12]

TiO_2 nanomaterials are extensively considered as state-of-the-art photocatalysts for energy conversion and environmental protection.[13–15] Nevertheless, the low photocatalytic performance caused by the large band gap, rapid recombination rate of photo-generated carriers and low specific surface area is a challenging issue which needs to be addressed to enable useful applications.[16,17] Structure engineering is a highly promising approach for improving the optical and electronic properties of TiO_2 in the visible light region.[18] For this aim, one way is deposition of noble metal particles on the surface of titania.[19] This noble metal grafting can efficiently increase the interfacial charge transfer by the formation of a "Schottky" barrier between titania and the metal, which can be indexed to various Fermi levels of the metal and TiO_2.[20] Under visible light illumination, the photo-induced electrons in the conduction band (CB) of titania can be transferred to noble metals as the Fermi level of these metal particles is located below the CB of the n-type TiO_2 semiconductor.[21]

On the other hand, Pd nanoparticles (NPs) play an important role in C–C bond-forming reactions due to their unique ability to activate reactants *via* the formation of metal–carbon bonds.[22] Although Pd NPs can strongly absorb UV and visible light through interband electronic transitions, their weak plasmonic properties inhibit the application of Pd in the plasmonic field.[12,23,24] With the help of the strong localized

[a] *Department of Chemistry, Faculty of Science, University of Alzahra, Tehran, Iran*
[b] *Department of Physical Chemistry, University of Geneva, 30 Quai Ernest-Ansermet, 1211, Geneva 4, Switzerland. E-mail: Thomas.Buergi@unige.ch; Tel: +41(0)22 379 65 52*
[c] *School of Chemistry, College of Science, University of Tehran, Tehran, Iran*
† Electronic supplementary information (ESI) available. See DOI: 10.1039/c9cy00798a

surface plasmon resonance (LSPR) of Au under light irradiation, Au/Pd bimetallic nanoparticles have been proven to be efficient in light harvesting and as catalysts for the Suzuki coupling reaction.[25–27] In this regard, several efforts have been devoted to improvement of the activity of heterogeneous AuPd-based TiO_2 catalysts for the visible-light-induced Suzuki coupling reaction. Yan *et al.* reported a well-designed Au–TiO_x–Pd photocatalyst that exhibited high performance towards Suzuki–Miyaura reactions under ambient conditions under solar irradiation.[28] Zhang and co-workers fabricated a Au–Pd/TiO_2 catalyst, which exhibited high photocatalytic activity for coupling reactions of aryl boronic acids with substituted aryl halides under visible light.[24] Inspired by these reports, we tried to design an engineered Au–Pd/TiO_2 architecture to improve the photocatalytic activity in the Suzuki reaction.

Among the various morphologies of TiO_2, yolk–shell (Y@S) structures, composed of a movable core inside a hollow cavity enclosed by a porous outer shell, have gained much research attention due to their unique properties.[29,30] These smart materials are conducive to photocatalysis due to their relatively high surface area, high light harvesting, low diffusion resistance and multiple light-scattering within the sphere interior voids.[30,31] To date, it has been demonstrated that nanoarchitectures with a hierarchical surface have enhanced features compared to those with a smooth surface.[32] Among them, readily accessible urchin-like structures with properties of an interconnected porous framework and high specific surface area can increase the efficiency of light harvesting as well as facilitate the accessibility of reactants to the active sites.[33] On the other hand, surface structure engineering has afforded many breakthroughs in enhancing the photocatalytic activity of titania through creating a defect-rich or disordered surface layer with black colour, therefore improving its optical absorption in the visible region.[34,35] The presence of oxygen vacancies on the surface of black TiO_2 provides excess electrons at the defect sites, decreases the band gap of TiO_2 to the visible region and decreases charge recombination.[24,36,37]

Based on the above considerations, the design of a noble metal NP decorated yolk–shell TiO_2 structure with a hydrogenated urchin-like surface is an effective method to solve the low light harvesting efficiency of titania which can lead to the next generation of advanced photocatalytic materials for coupling reactions. Therefore, following research endeavours from our groups,[38–41] herein we wish to propose a hierarchical urchin-like yolk@shell TiO_2 architecture decorated with plasmonic Au/Pd NPs (HUY@S-TOH@AuPd) as an advanced architecture for photocatalytic Suzuki–Miyaura coupling reactions at room temperature under visible light irradiation.

Results and discussion

Preparation and characterization of the HUY@S-TOH/AuPd architecture

Fig. 1 illustrates the multi-step procedure for the preparation of HUY@S-TOH/AuPd nanoarchitectures. In step I, the Y@S-TO spheres are formed by a one-pot solvothermal method using polyethylene glycol as a soft template.[40] Next, in step II, a dissolution–recrystallization process in an alkaline water/alcohol medium was used to produce the hierarchical urchin like shell (HUY@S-TO). In step III, the 3D HUY@S-TOH architectures were obtained by using a hydrogen treatment method.[42] Finally, the as-prepared Au/Pd core/shell NPs were decorated on the surface of HUY@S-TOH to yield the HUY@S-TOH/AuPd architecture (step IV).

SEM analysis was used to investigate the surface morphology of the designed architecture. The SEM image of HUY@S-TOH/AuPd (Fig. 2a) shows the presence of urchin-like monodisperse microspheres with a diameter of ~3 μm. The broken sphere (yellow arrow) implies the Y@S configuration in which a movable solid core was located inside the urchin-like shell. From the SEM images of HUY@S-TOH/AuPd at higher magnifications (Fig. 2b and c), the well-developed hairy needles assembled on the surface of the microspheres are clearly seen, resulting in urchin-like structures.

More detailed morphological information of the designed structures was obtained by TEM analysis in comparison with the Y@S-TO structure. The typical TEM images of Y@S-TO (Fig. 3a–c) at different magnifications confirmed the Y@S configuration in this structure. Moreover, the relatively smooth surface in this structure is clearly obvious (Fig. 3c). Besides, Fig. 3(f–h) revealed the hierarchical urchin-like structure of HUY@S-TOH that was created by the dissolution–recrystallization process in a water/alcohol medium. As can be seen in these images, the urchin-like needles were successfully assembled on the surface of the Y@S structure.

High-resolution TEM (HRTEM) images of Y@S-TO (Fig. 4a and b) and HUY@S-TOH/AuPd (Fig. 4c and d) clearly indicate that the two structures have good crystallinity with an interplanar distance of 0.35 nm between (101) TiO_2 planes (red arrows). Meanwhile, in the case of the HUY@S-TOH/AuPd architecture, a thin disordered surface layer (white arrows) owing to the effect of hydrogen treatment could be observed.[43] Additionally, in Fig. 4c and d, spherical AuPd NPs are evident on the surface needles of the HUY@S-TOH architecture with an average diameter of ~5 nm and a lattice

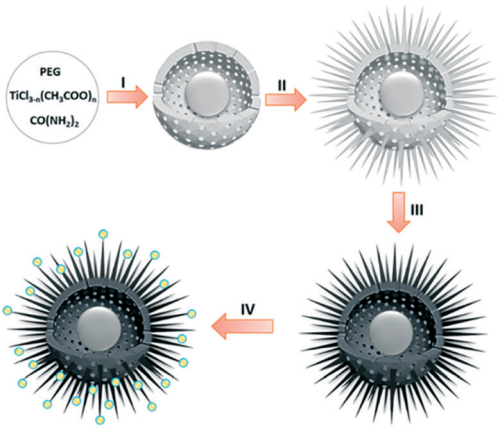

Fig. 1 Overall flowchart for the fabrication of the HUY@S-TOH/AuPd architecture.

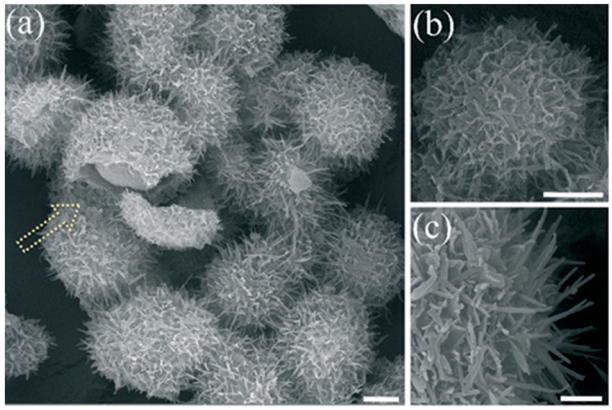

Fig. 2 SEM images of the HUY@S-TOH/AuPd architecture. The scale bars are 1 μm (a and b) and 200 nm (c).

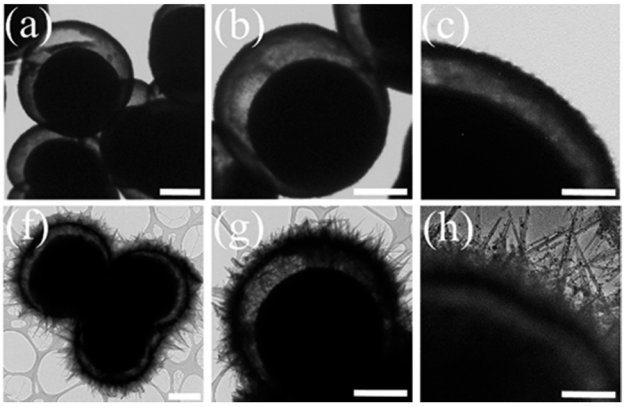

Fig. 3 TEM images of Y@S-TO (a–c) and HUY@S-TOH/AuPd (f–h). The scale bars are 1 μm (a, b, f and g) and 200 nm (c and h).

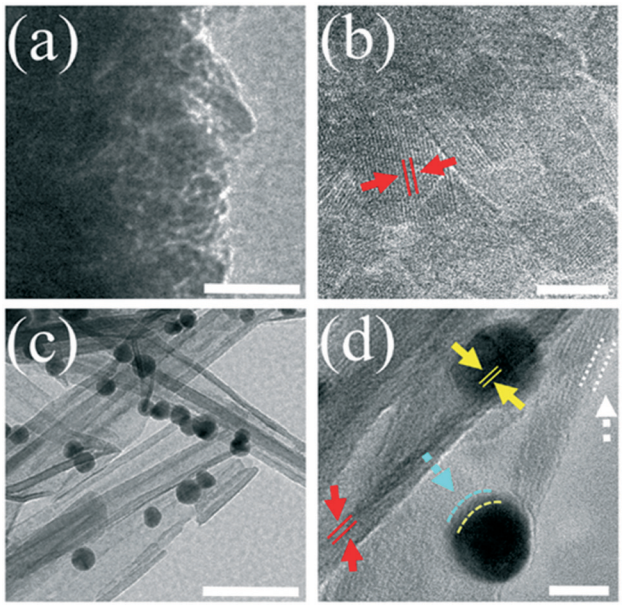

Fig. 4 HRTEM images of Y@S-TO (a and b) and HUY@S-TOH/AuPd (c and d). The scale bars are 50 nm (a and c) and 5 nm (b and d).

spacing of about 0.24 nm, which matched well with the (111) crystalline plane of Au (yellow arrows). A narrow shell on the surface of Au NPs (blue line, *ca.* 0.7 nm) is obvious, which can be attributed to the Pd deposition and preparation of Au–Pd core/shell NPs, as later on confirmed by XPS analysis. Moreover, to better distinguish the structure of Au and Pd, HRTEM analysis was done for pristine AuPd nanoparticles. As is clear from Fig. S1,† the Au core (darker part) is covered by the Pd shell (lighter part).

Energy dispersive X-ray spectroscopy (EDS) elemental mapping analysis was also performed to identify the elemental composition of the architecture (Fig. S2†). The results reveal that the HUY@S-TOH/AuPd structure mainly contains a uniform distribution of Ti, O and Au as well as Pd elements.

X-ray photoelectron spectroscopy (XPS) was used to analyze the valence states of Ti, Pd and Au in the modified HUY@S-TOH/AuPd architecture (Fig. S3†). As can be seen in Fig. S3a,† the two bands located at binding energies (BEs) of 459.0 eV and 464.9 eV were attributable to the Ti $2p_{3/2}$ and Ti $2p_{1/2}$ photoelectrons in the Ti^{4+} chemical state, while the two peaks at 456.9 eV and 463.2 eV were indexed to the $2p_{3/2}$ and $2p_{1/2}$ core levels of Ti^{3+} in the black TiO_2. Besides, the Au 4f and Pd 3d spectra showed two contributions resulting from spin–orbit splitting. The BE peak at 83.2 eV corresponds to Au $4f_{7/2}$, suggesting the presence of Au (0) species on the surface of the nanoarchitecture.[44] Meanwhile, the main BE peak of Pd $3d_{5/2}$ was located at 333.7 eV, suggesting that the Pd species are in a metallic state which has been proven efficient for attaining high catalytic performance toward the Suzuki coupling reaction. Remarkably, a slight positive shift relative to the typical BE of Ti $2p_{3/2}$ at 459.0 eV and also a negative shift of the typical BE for Au (0) and Pd (0) at 84.0 eV and 335.0 eV, respectively, can be attributed to the transfer of electrons from the titania to the Au/Pd core/shell nanospheres.[24,45,46] These electron flows can enhance the electron density around the Pd particles which can accelerate the Suzuki reaction. Besides, the weight amounts of the Au and Pd species in the engineered HUY@S-TOH/AuPd structure, determined by XPS analysis, are ~2.3 and 0.6 wt% respectively.

XRD and DRS analyses of Y@S-TO, HUY@S-TOH and HUY@S-TOH/AuPd were also performed (Fig. S4†). The XRD patterns confirmed that all the architectures possess good crystallinity with a well-defined tetragonal anatase structure of TiO_2 (JCPDS No. 21-1272). After hydrogenation, a slight shift to higher diffraction angles was observed in HUY@S-TOH which can be attributed to the reduction of the interplanar spacing of the crystalline titania phase.[47] In the engineered HUY@S-TOH/AuPd structure, all the reflections are preserved, implying that the decoration with Au–Pd NPs has no effect on the crystal phase of the TiO_2 support. Moreover, two small reflections could be observed at ~38° and 44° for the (111) and (200) planes of Au, respectively (JCPDS: 10-0784). No distinct diffraction peaks ascribed to Pd are distinguished, because the size of the Pd shell deposited on the surface of the Au core is lower than the detection limit of

XRD analysis (<4 nm). Evidence for the formation of Ti^{3+} and Au–Pd core–shell NPs on the engineered structure was also seen by UV-vis diffuse reflectance spectroscopy (DRS) in which the HUY@S-TOH/AuPd architecture clearly demonstrated different features from the HUY@S-TOH and Y@S-TO structures. As shown in Fig. S5,† Y@S-TO displayed great light absorption at wavelengths above 400 nm. In contrast, the spectrum of HUY@S-TOH shows significant absorption of visible light that may be due to the presence of Ti^{3+} ions on the surface of the structure. After decoration with Au–Pd, an even stronger absorption in the visible region was observed for the modified HUY@S-TOH/AuPd architecture. The strong peak at ~532 nm is due to the LSPR effect of the core/shell Au–Pd NPs.[46]

N_2 adsorption–desorption measurement was conducted to investigate the porous structure and pore size distribution of the HUY@S-TOH/AuPd sample (Fig. S6†). Unlike P25, which is not mesoporous, for the Y@S-TO and HUY@S-TOH/AuPd architectures, typical type IV isotherms are observed, indicating the presence of mesopores in these structures. Thanks to the advantage of the urchin-like surface as well as the Y@S structure, the BET surface area of HUY@S-TOH/AuPd (306 $m^2\ g^{-1}$) is nearly two times larger than that of Y@S-TO (181 $m^2\ g^{-1}$) and much larger than that of P25 (41 $m^2\ g^{-1}$). This high surface area is desirable for great adsorption of organic substrates and efficient anchoring of AuPd NPs leads to an improved photocatalytic coupling reaction. According to Barrett–Joyner–Halenda (BJH) analysis, the HUY@S-TOH/AuPd structure presented a narrow pore-size distribution in the range of 2–8 nm (Fig. S7†).

Photocatalytic investigations

The influence of some critical reaction conditions in Suzuki coupling has been investigated by using the HUY@S-TOH/AuPd photocatalyst under 300 W xenon lamp irradiation, as simulated sunlight, at room temperature. The Suzuki reaction between 4-iodotoluene with phenylboronic acid, as a model reaction, did not proceed in the dark (Table S1,† entry 1) and at 80 °C (in the dark) a moderate yield (68%) of the corresponding product was observed (Table S1,† entry 2), indicating the significant influence of irradiation on the catalytic performance. Among the several solvents that were used for the reaction, polar aprotic solvents, such as DMF and DMSO, gave low yields of the product and the nonpolar solvent toluene also afforded a trace yield (Table S1,† entries 3–5). In contrast, higher yields of the product were observed in polar protic solvents like ethanol and methanol (Table S1,† entries 6 and 7). In addition, the reaction in pure H_2O hardly proceeded because of the poor solubility of 4-iodotoluene at room temperature (Table S1,† entry 8); however, a mixture of protic EtOH and H_2O led to a profound increase in catalytic activity (Table S1,† entry 13). This result is very different from that obtained in conventional Suzuki coupling reactions catalyzed by heterogeneous catalysts. Generally, polar DMSO and DMF are considered to be good solvents for Suzuki coupling, leading to the generation of the corresponding products in high yields. Nevertheless, this is not the case for photocatalyzed Suzuki coupling reactions. Additionally, another protic organic solvent mixture involving MeOH gave moderate yields of the desired product in this photocatalyzed coupling reaction. These results confirmed that protic solvents play a crucial role in photocatalyzed Suzuki reactions over the HUY@S-TOH/AuPd nanocatalyst. It is hypothesized that protic solvents may be oxidized more easily through photogenerated holes transferred from Y@S-TO. In contrast, aprotic solvents like DMSO and DMF could not be oxidized by this hole transfer since they have higher oxidation potentials.[48] Subsequently, the effects of various bases in the mixture of EtOH : H_2O were investigated and the best result was obtained using K_2CO_3 (Table S1,† entry 13). Moreover, the reaction did not proceed without a base (Table S1,† entry 15), as it is necessary to activate the phenylboronic acid and it facilitates the transmetalation step.[49] Besides, different loadings of Au/Pd nanoparticles on the HUY@S-TOH architecture were investigated in the Suzuki model reaction (Fig. S8†). As seen from the data, the best result was obtained using 3 wt% Au/Pd. By increasing the metal loading beyond 3 wt%, no considerable improvements in product yields were observed. To obtain better insight into the HUY@S-TOH/AuPd nanoarchitecture efficiency, its photocatalytic activity in the model reaction under optimized conditions was compared with that of P-25, P-25/AuPd, Y@S-TO/AuPd, HUY@S-TOH/Au, HUY@S-TOH/Pd and HUY@S-TOH/AuPd structures. As can be seen in Fig. S9,† by using P-25, the reaction did not proceed at all probably due to the lack of visible light activity as well as the absence of metal NPs in this structure. However, the activity of the catalyst is significantly improved with the decoration of Au–Pd nanoparticles on the structures, with the yield of the reaction being increased to 69% and 78% after 1 h using P-25/AuPd and Y@S-TO/AuPd, respectively. The higher photocatalytic activity of Y@S-TO/AuPd compared to that of P25/AuPd can be ascribed to its higher surface area and better light harvesting ability, provided by the yolk/shell structure in Y@S-TO/AuPd. By using monometallic structures, HUY@S-TOH/Au gave only little product (17%) and HUY@S-TOH/Pd demonstrated inferior activity compared with HUY@S-TOH/AuPd, as the yield of the product was only 43%. This implies that the presence of both Au and Pd plays an important role in this photocatalytic reaction. Interestingly, the highest photocatalytic activity was observed using the HUY@S-TOH/AuPd architecture with a product yield of 94% in 1 h. This considerable activity can be attributed to the hydrogenated visible light active structure containing Ti^{3+} species on the surface of TiO_2. The latter enhance the light harvesting efficiency of photocatalysts through inhibition of the recombination of photo-generated electrons and holes by decreasing the band gap of TiO_2 to the visible region. Furthermore, scattering of light on the hierarchical surface and between the inner core and outer shell in the urchin-like Y@S structure can enhance the light harvesting efficiency. Moreover, the results indicate the strong interaction between noble metals and TiO_{2-x}. Electron transfer between Ti^{3+} and metal particles, as

previously verified by XPS analysis, leads to an electron-rich Pd surface, which finally increases the catalytic performance of this architecture.[50] These results clearly demonstrate the high activity of the used urchin-like hydrogenated HUY@S-TOH/AuPd nanoarchitecture for the photocatalytic Suzuki coupling reaction. The reaction protocol was further extended to the coupling of different aryl halides and phenylboronic acids to confirm the scope of the catalytic system HUY@S-TOH/AuPd under visible light irradiation (Table 1). As expected, in the case of aryl iodides, the corresponding biaryls were obtained in higher yields than aryl bromides and chlorides due to the weaker C–I bond. Moreover, the electronic nature of the substituents on the phenyl rings can affect the yield of the desired products. Aryl halides with electron withdrawing substituents exhibited higher product yields as compared to those with electron donating ones. This result is reasonable, since the electron withdrawing substituents result in an electron deficient aromatic ring which facilitates the nucleophilic attack *via* the photo-induced electrons on the electron-rich Pd NPs. To better visualize the effect of different aryl halides on the reaction rate of Suzuki coupling, the yields of some bromobenzenes *vs.* Hammett's parameters are shown in Fig. S10.† To avoid complications caused by steric hindrance effects, a Hammett plot was constructed for substituents in the *para*-position. As expected, in the presence of electron-withdrawing groups at *para*-substituted bromobenzenes, the yields of biphenyls were enhanced.[51,52] These results are concurrent when correlated with the Hammett parameter values.[53]

Furthermore, *meta*-substituted aryl halides showed lower activity than those with *para*- and *ortho*-substituents, probably a consequence of both steric hindrance and electronic effects (Table 1, 3g–i).

To get insight into the mechanism responsible for the photocatalyzed Suzuki reaction using the HUY@S-TOH/AuPd architecture, the coupling of 4-iodotoluene with phenylboronic acid in the presence of electron and hole scavengers was studied. 5,5-Dimethyl-1-pyrroline *N*-oxide (DMPO) was used as an electron scavenger to trap the electrons from Pd, which can activate 4-iodotoluene.[54] With addition of DMPO, no desired product was observed, suggesting that the coupling reaction could not proceed without the reduction by the electrons from Pd. Next, the role of photo-generated holes from the nanoarchitecture was investigated. Phenylboronic acid can combine with OH^- ions in basic solution and in principle adsorb on TiO_2 *via* electrostatic interaction. The photo-induced holes can diffuse to the adsorption sites of phenylboronic acid, and the adsorbed molecules could be oxidized with the cleavage of the C–B bond.[28] Therefore, phenylboronic acid can be activated *via* photo-generated holes under visible light illumination. To demonstrate this, triethanolamine (TEOA) as a hole scavenger was used in the same reaction. It was observed that the reaction was quenched. Even though these results demonstrate the importance of the electron–hole pair in the photocatalytic Suzuki reaction, the exact role of holes is not yet clear.[55,56]

Based on the above experimental results and mechanistic studies, a plausible photocatalytic mechanism can be proposed for the Suzuki–Miyaura coupling over the HUY@S-TOH/AuPd photocatalyst (Fig. 5). Under irradiation of visible light, hydrogenated titania can absorb part of the visible light and produce electron–hole pairs. The photo-induced electrons can be injected into Au/Pd nanoparticles.[57] In parallel, the produced hot electrons, resulting from the strong LSPR effect of Au, could be injected into the Pd shell to

Table 1 Scope of the Suzuki coupling reaction catalyzed by HUY@S-TOH/AuPd under visible-light irradiation[a]

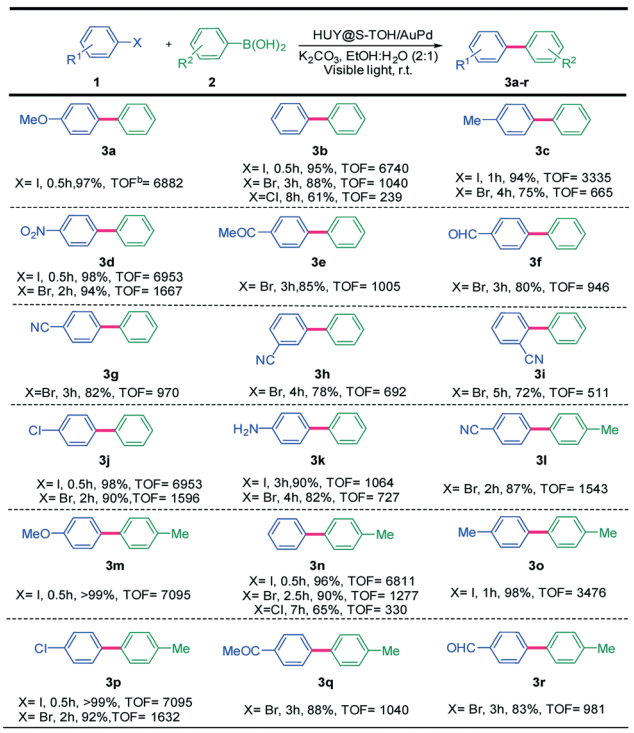

[a] Reaction conditions: aryl halide (1.0 mmol), phenylboronic acids (1.5 mmol), HUY@S-TOH/AuPd catalyst (5 mg), K_2CO_3 (2 mmol) and EtOH : H_2O (6 mL), Xe lamp, water bath, room temperature. Yields refer to isolated pure compounds. [b] TOF (h^{-1}) is calculated based on the yield of products and the number of moles of Pd used.

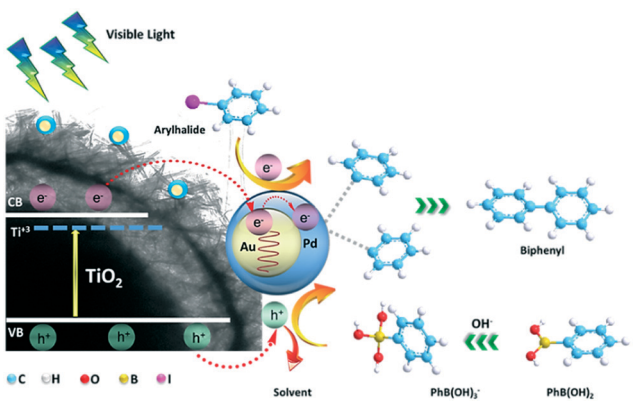

Fig. 5 Plausible mechanism for the visible light induced photocatalytic Suzuki–Miyaura coupling reaction using HUY@S-TOH/AuPd.

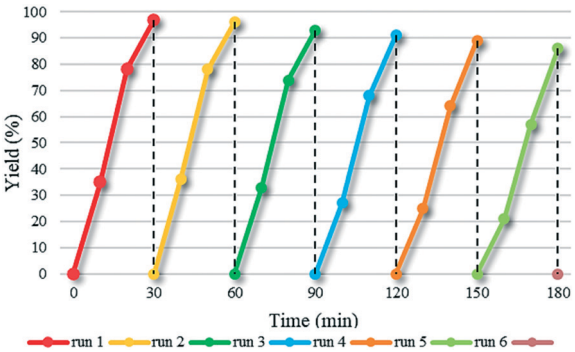

Fig. 6 Reusability study of HUY@S-TOH/AuPd in the photocatalytic Suzuki coupling reaction of 4-iodoanisole and phenylboronic acid.

increase the electron density of Pd.[58] Subsequently, the electron-rich Pd NPs can activate the C–X bond of aryl halides and facilitate the oxidative addition step that seems to be the rate-determining step of the Suzuki reaction. On the other hand, the photo-generated holes can transfer to the protic organic solvent, such as EtOH, or can activate phenylboronic acid by cleaving the C–B bonds.[56,59] When the oxidized phenylboronic acids transfer to the activated aryl halides, the cross-coupling reaction occurs to produce the desired products *via* reductive elimination.

Photo-stability and reusability tests, as important characteristics in photocatalytic reactions, were performed to explore the stability of the designed architecture. After photocatalytic Suzuki coupling of 4-iodoanisole and phenylboronic acid, the HUY@S-TOH/AuPd photocatalyst was separated from the reaction solution by centrifugation, washed with hot EtOH, and then reused for the same reaction. As can be clearly observed in Fig. 6, the nanoarchitecture exhibited high catalytic performance for six cycles without a significant loss of activity (every run is completed in 30 min).

A comparison reveals the highest TOF for the engineered HUY@S-TOH/AuPd nanoarchitecture in the photocatalytic Suzuki reaction with respect to other reports. As can be seen in Fig. 7 and Table S1,†[24,28,54–57,59–64] our catalyst has the best performance reported to date (TOF = 7095 h^{-1}). The good performance of the hydrogenated visible light active architecture can be attributed to the urchin-like surface structure that provides a more accessible surface area for higher Au–Pd anchoring, preventing the agglomeration of Pd species during catalytic cycles.

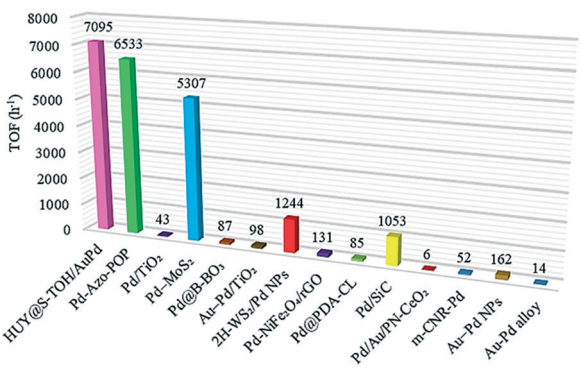

Fig. 7 Comparison of the maximum TOF value of HUY@S-TOH/AuPd with those of previously published catalysts for visible-light Suzuki reactions.

Conclusions

In conclusion, we report an engineered design for the synthesis of the HUY@S-TOH/AuPd architecture which demonstrated excellent photocatalytic activity in visible-light-promoted Suzuki coupling reactions under ambient conditions. The improved activity of the catalyst can be attributed to the hierarchical structure with a high accessible surface area, numerous anchoring sites for Au/Pd, efficient light harvesting in the urchin-like Y@S structure, and considerable photon absorption efficiency of visible light due to the existence of oxygen vacancies as well as noble metal NPs. Moreover, the cooperative promoting effect between plasmonic Au and Pd NPs is an effective way for transferring energetic electrons from gold to palladium by the LSPR effect. A mechanistic investigation of the photocatalytic Suzuki reaction suggested that photo-induced holes are transferred into EtOH or phenylboronic acid, whereas photo-generated electrons are injected into Pd NPs which can accelerate the coupling reaction. This synthetic approach for structuring Au/Pd NPs on the surface of hydrogenated titania in advanced architectures can be extended to the rational design of structures with greatly improved photocatalytic activity for various energy applications and also other cross-coupling reactions using visible light.

Conflicts of interest

There are no conflicts to declare.

Acknowledgements

The financial support from the research council of Alzahra University, the University of Geneva, and the University of Tehran is gratefully acknowledged. SR would like to thank Ani Baghdasaryan for her help in NMR measurements.

References

1 X. Lang, X. Chen and J. Zhao, *Chem. Soc. Rev.*, 2014, **43**, 473–486.
2 M. Parasram and V. Gevorgyan, *Chem. Soc. Rev.*, 2017, **46**, 6227–6240.
3 J. C. Colmenares and R. Luque, *Chem. Soc. Rev.*, 2014, **43**, 765–778.
4 X.-H. Li, J.-S. Chen, X. Wang, J. Sun and M. Antonietti, *J. Am. Chem. Soc.*, 2011, **133**, 8074–8077.
5 C. C. Nguyen, N. N. Vu and T.-O. Do, *J. Mater. Chem. A*, 2015, **3**, 18345–18359.
6 J. Kou, C. Lu, J. Wang, Y. Chen, Z. Xu and R. S. Varma, *Chem. Rev.*, 2017, **117**, 1445–1514.

7 N. Miyaura, K. Yamada and A. Suzuki, *Tetrahedron Lett.*, 1979, **20**, 3437–3440.
8 N. Miyaura and A. Suzuki, *Chem. Rev.*, 1995, **95**, 2457–2483.
9 A. J. Lennox and G. C. Lloyd-Jones, *Chem. Soc. Rev.*, 2014, **43**, 412–443.
10 Q. Wu, P. Ju, S. Wu, Q. Su, X. Li, Z. Liu and G. Li, *J. Mater. Chem. A*, 2019, **7**, 2660–2666.
11 H. H. Shin, T. Han, W. Yang and D.-K. Lim, *Carbon*, 2019, **143**, 362–370.
12 Y. Zhang, S. He, W. Guo, Y. Hu, J. Huang, J. R. Mulcahy and W. D. Wei, *Chem. Rev.*, 2017, **118**, 2927–2954.
13 M. Pelaez, N. T. Nolan, S. C. Pillai, M. K. Seery, P. Falaras, A. G. Kontos, P. S. Dunlop, J. W. Hamilton, J. A. Byrne and K. O'shea, *Appl. Catal., B*, 2012, **125**, 331–349.
14 J. Schneider, M. Matsuoka, M. Takeuchi, J. Zhang, Y. Horiuchi, M. Anpo and D. W. Bahnemann, *Chem. Rev.*, 2014, **114**, 9919–9986.
15 D. Ma, A. Liu, S. Li, C. Lu and C. Chen, *Catal. Sci. Technol.*, 2018, **8**, 2030–2045.
16 W. Fang, M. Xing and J. Zhang, *J. Photochem. Photobiol., C*, 2017, **32**, 21–39.
17 M. Ge, C. Cao, J. Huang, S. Li, Z. Chen, K.-Q. Zhang, S. Al-Deyab and Y. Lai, *J. Mater. Chem. A*, 2016, **4**, 6772–6801.
18 M. Nasr, C. Eid, R. Habchi, P. Miele and M. Bechelany, *ChemSusChem*, 2018, **11**, 3023–3047.
19 Y. Chen, Y. Wang, W. Li, Q. Yang, Q. Hou, L. Wei, L. Liu, F. Huang and M. Ju, *Appl. Catal., B*, 2017, **210**, 352–367.
20 O. Ola and M. M. Maroto-Valer, *J. Photochem. Photobiol., C*, 2015, **24**, 16–42.
21 J. B. Joo, H. Liu, Y. J. Lee, M. Dahl, H. Yu, F. Zaera and Y. Yin, *Catal. Today*, 2016, **264**, 261–269.
22 A. Biffis, P. Centomo, A. Del Zotto and M. Zecca, *Chem. Rev.*, 2018, **118**, 2249–2295.
23 T. Pakizeh, *J. Opt.*, 2012, **15**, 025001.
24 D. Han, Z. Bao, H. Xing, Y. Yang, Q. Ren and Z. Zhang, *Nanoscale*, 2017, **9**, 6026–6032.
25 K. D. Gilroy, A. Ruditskiy, H.-C. Peng, D. Qin and Y. Xia, *Chem. Rev.*, 2016, **116**, 10414–10472.
26 M. Wen, S. Takakura, K. Fuku, K. Mori and H. Yamashita, *Catal. Today*, 2015, **242**, 381–385.
27 N. A. Nemygina, L. Z. Nikoshvili, I. Y. Tiamina, A. V. Bykov, I. S. Smirnov, T. LaGrange, Z. Kaszkur, V. G. Matveeva, E. M. Sulman and L. Kiwi-Minsker, *Org. Process Res. Dev.*, 2018, **22**, 1606–1613.
28 F. Wang, C. Li, H. Chen, R. Jiang, L.-D. Sun, Q. Li, J. Wang, J. C. Yu and C.-H. Yan, *J. Am. Chem. Soc.*, 2013, **135**, 5588–5601.
29 R. Purbia and S. Paria, *Nanoscale*, 2015, **7**, 19789–19873.
30 J. Liu, S. Z. Qiao, J. S. Chen, X. W. D. Lou, X. Xing and G. Q. M. Lu, *Chem. Commun.*, 2011, **47**, 12578–12591.
31 Z. Li, M. Li, Z. Bian, Y. Kathiraser and S. Kawi, *Appl. Catal., B*, 2016, **188**, 324–341.
32 X. Li, J. Yu and M. Jaroniec, *Chem. Soc. Rev.*, 2016, **45**, 2603–2636.
33 J. Jiang, Z. Xing, M. Li, Z. Li, X. Wu, M. Hu, J. Wan, N. Wang, A. S. Besov and W. Zhou, *Ind. Eng. Chem. Res.*, 2017, **56**, 7948–7956.
34 W. Zhou, W. Li, J.-Q. Wang, Y. Qu, Y. Yang, Y. Xie, K. Zhang, L. Wang, H. Fu and D. Zhao, *J. Am. Chem. Soc.*, 2014, **136**, 9280–9283.
35 L.-B. Xiong, J.-L. Li, B. Yang and Y. Yu, *J. Nanomater.*, 2012, **2012**, 9.
36 A. Ziarati, A. Badiei and R. Luque, *Appl. Catal., B*, 2018, **238**, 177–183.
37 X. Chen, L. Liu and F. Huang, *Chem. Soc. Rev.*, 2015, **44**, 1861–1885.
38 S. Rohani, G. Mohammadi Ziarani, A. Badiei, A. Ziarati, M. Jafari and A. Shayesteh, *Appl. Organomet. Chem.*, 2018, e4397.
39 A. Ziarati, A. Badiei, R. Grillo and T. Burgi, *ACS Appl. Mater. Interfaces*, 2019, **11**, 5903–5910.
40 A. Ziarati, A. Badiei, R. Luque and W. Ouyang, *J. Mater. Chem. A*, 2018, **6**, 8962–8968.
41 A. Ziarati, A. Badiei and R. Luque, *Appl. Catal., B*, 2019, **240**, 72–78.
42 D. Chen, C. Li, H. Liu, F. Ye and J. Yang, *Sci. Rep.*, 2015, **5**, 11949.
43 X. Chen, L. Liu, Y. Y. Peter and S. S. Mao, *Science*, 2011, 1200448.
44 P. Saikia, A. T. MIAH and P. P. Das, *J. Chem. Sci.*, 2017, **129**, 81–93.
45 A. Cybula, J. B. Priebe, M.-M. Pohl, J. W. Sobczak, M. Schneider, A. Zielińska-Jurek, A. Brückner and A. Zaleska, *Appl. Catal., B*, 2014, **152**, 202–211.
46 C. Han, L. Wu, L. Ge, Y. Li and Z. Zhao, *Carbon*, 2015, **92**, 31–40.
47 T. Xia and X. Chen, *J. Mater. Chem. A*, 2013, **1**, 2983–2989.
48 O. R. Luca, J. L. Gustafson, S. M. Maddox, A. Q. Fenwick and D. C. Smith, *Org. Chem. Front.*, 2015, **2**, 823–848.
49 Y. Q. Zou, J. R. Chen, X. P. Liu, L. Q. Lu, R. L. Davis, K. A. Jørgensen and W. J. Xiao, *Angew. Chem.*, 2012, **124**, 808–812.
50 X. Yuan, X. Wang, X. Liu, H. Ge, G. Yin, C. Dong and F. Huang, *ACS Appl. Mater. Interfaces*, 2016, **8**, 27654–27660.
51 F. Estudiante-Negrete, S. Hernández-Ortega and D. Morales-Morales, *Inorg. Chim. Acta*, 2012, **387**, 58–63.
52 J. R. Pioquinto-Mendoza, P. Conelly-Espinosa, R. Reyes-Martínez, R. A. Toscano, J. M. Germán-Acacio, A. Avila-Sorrosa, O. Baldovino-Pantaleón and D. Morales-Morales, *J. Organomet. Chem.*, 2015, **797**, 153–158.
53 C. Hansch, A. Leo and R. Taft, *Chem. Rev.*, 1991, **91**, 165–195.
54 Z. Jiao, Z. Zhai, X. Guo and X.-Y. Guo, *J. Phys. Chem. C*, 2015, **119**, 3238–3243.
55 X.-H. Li, M. Baar, S. Blechert and M. Antonietti, *Sci. Rep.*, 2013, **3**, 1743.
56 F. Raza, D. Yim, J. H. Park, H.-I. Kim, S.-J. Jeon and J.-H. Kim, *J. Am. Chem. Soc.*, 2017, **139**, 14767–14774.
57 S. Zhang, C. Chang, Z. Huang, Y. Ma, W. Gao, J. Li and Y. Qu, *ACS Catal.*, 2015, **5**, 6481–6488.
58 P. Verma, Y. Kuwahara, K. Mori and H. Yamashita, *J. Mater. Chem. A*, 2016, **4**, 10142–10150.

59 H. H. Shin, E. Kang, H. Park, T. Han, C.-H. Lee and D.-K. Lim, *J. Mater. Chem. A*, 2017, **5**, 24965–24971.
60 J. Chakraborty, I. Nath and F. Verpoort, *Chem. Eng. J.*, 2019, **358**, 580–588.
61 Z. J. Wang, S. Ghasimi, K. Landfester and K. A. Zhang, *Chem. Mater.*, 2015, **27**, 1921–1924.
62 Y. Li, Z. Zhang, L. Pei, X. Li, T. Fan, J. Ji, J. Shen and M. Ye, *Appl. Catal., B*, 2016, **190**, 1–11.
63 A. Xie, K. Zhang, F. Wu, N. Wang, Y. Wang and M. Wang, *Catal. Sci. Technol.*, 2016, **6**, 1764–1771.
64 Q. Xiao, S. Sarina, E. Jaatinen, J. Jia, D. P. Arnold, H. Liu and H. Zhu, *Green Chem.*, 2014, **16**, 4272–4285.